1521-009X/52/5/368–376$35.00
DRUG METABOLISM AND DISPOSITION

dx.doi.org/10.1124/dmd.123.001611
Drug Metab Dispos 52:368–376, May 2024

Identification and Biosynthesis of an *N*-Glucuronide Metabolite of Camonsertib[S]

Robert Papp, Laird Trimble, Adrian J. Fretland, Ravi Manohar, Richard Phipps, Lisbet Kvaerno, Alexander L. Perryman, Gregory Reynolds, and W. Cameron Black

Repare Therapeutics, Saint-Laurent, Quebec, Canada (R.Pa., A.L.P., W.C.B.); Repare Therapeutics, Cambridge, Massachusetts (A.J.F.); Trimble Analytical Services, Ottawa, Ontario, Canada (L.T.); Hypha Discovery, Abingdon, United Kingdom (R.M., R.Ph., L.K.); and BioAgilytix, San Diego, California (G.R.)

Received December 1, 2023; accepted February 14, 2024

ABSTRACT

Camonsertib is a novel ATR kinase inhibitor in clinical development for advanced cancers targeting sensitizing mutations. This article describes the identification and biosynthesis of an *N*-glucuronide metabolite of camonsertib. This metabolite was first observed in human hepatocyte incubations and was subsequently isolated to determine the structure, evaluate its stability as part of bioanalytical method development and for use as a standard for estimating its concentration in phase I samples. The *N*-glucuronide was scaled-up using a purified bacterial culture preparation and was subsequently isolated using preparative chromatography. The bacterial culture generated sufficient material of the glucuronide to allow for one- and two-dimensional ^{1}H and ^{13}C NMR structural elucidation and further bioanalytical characterization. The nuclear Overhauser effect data combined with the gradient heteronuclear multiple bond correlation experiment and molecular modeling, strongly suggests that the point of attachment of the glucuronide results in the formation of (2*S*,3*S*,4*S*,5*R*,6*R*)-3,4,5-trihydroxy-6-(5-(4-((1*R*,3*r*,5*S*)-3-hydroxy-8-oxabicyclo[3.2.1]octan-3-yl)-6-((*R*)-3-methylmorpholino)-1*H*-pyrazolo[3,4-*b*]pyridin-1-yl)-1*H*-pyrazol-1-yl)tetrahydro-2*H*-pyran-2-carboxylic acid.

SIGNIFICANCE STATEMENT

This is the first report of a glucuronide metabolite of camonsertib formed by human hepatocyte incubations. This study reveals the structure of an *N*-glucuronide metabolite of camonsertib using detailed elucidation by one- and two-dimensional NMR after scale-up using a novel bacterial culture approach yielding significant quantities of a purified metabolite.

Introduction

Direct glucuronidation of drugs is an important metabolic clearance mechanism and results from enzymatic conjugation with uridine diphosphate glucuronic acid by UDP-glucuronosyltransferases (UGT) enzymes. Typical functional groups known to be substrates of direct glucuronidation include carboxylic acids, hydroxyls, amines (Sadeque et al., 2012), and nitrogen heterocycles (Kaivosaari et al., 2011), whereas less common examples include carbon (Kerdpin et al., 2006) and sulfur glucuronides (Keating et al., 2006). Glucuronide metabolites can be unstable, hydrolyzing back to the parent drug under physiological conditions, including biological fluids such as plasma or urine (Yuan et al., 2020) or to a lesser extent in tissues (Yang et al., 2017). Additionally, acyl-glucuronides can undergo acyl migration leading to formation of a reactive intermediate, which can lead to potential protein binding through a glycation mechanism (Bailey and Dickinson 2003). Therefore, prediction or characterization of acyl reactivity rates can mitigate issues arising from instability or reactivity (Bradshaw et al., 2020).

Metabolite identification studies are an important part of the overall understanding of drug disposition and can identify potential safety concerns related to disproportionate metabolites that may appear in humans. Preclinical metabolite studies are generally used to guide chemistry efforts to reduce metabolic clearance, but they can also help highlight risks to bioanalytical methods arising from potentially unstable metabolites, which can interfere with accurate quantitation of the parent compound. For example, bioanalysis of muraglitazar described an acidification step during collection of the plasma to prevent the hydrolysis of the glucuronide to the aglycone, which would confound bioanalytical results and pharmacokinetic estimates (Wang et al., 2006). Early knowledge of such information is particularly valuable prior to or during formal method validations and laboratory preparations for first-in-human studies.

Camonsertib is a novel and selective ATR inhibitor currently in development for advanced solid tumor cancers (Roulston et al., 2022; Yap et al., 2023). Metabolite identification studies using human hepatocytes in suspension revealed the presence of a glucuronide metabolite (+176 atomic mass unit [amu]) using high resolution mass spectrometry. According to Fig. 1, camonsertib contains several potential sites of glucuronidation, including multiple heterocyclic nitrogen atoms, as well as a tertiary alcohol. To definitively identify the location of the camonsertib glucuronide, it was necessary to generate and isolate appropriate amounts needed for NMR structure elucidation. Several approaches were evaluated including chemical synthesis, incubations with liver

All studies were funded by Repare Therapeutics.
The authors from Repare Therapeutics may hold stock in the company.
dx.doi.org/10.1124/dmd.123.001611.
[S] This article has supplemental material available at dmd.aspetjournals.org.

ABBREVIATIONS: amu, atomic mass unit; COSY, correlated spectroscopy; HMBC, heteronuclear multiple bond correlation; HPLC, high-performance liquid chromatograph; HSQC, heteronuclear single quantum coherence; LC-MS/MS, liquid chromatography tandem mass spectrometry; NOE, nuclear Overhauser effect; NOESY, nuclear Overhauser enhancement spectroscopy; ROESY, rotating frame Overhauser enhancement spectroscopy; UGT, UDP-glucuronosyl transferases.

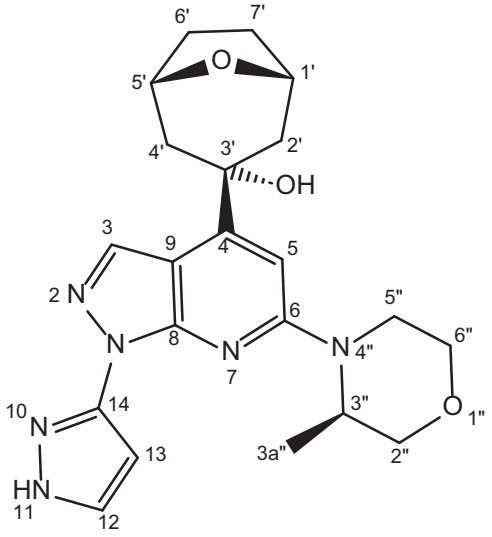

Fig. 1. Chemical structure of camonsertib.

subcellular fractions, fungal and bacterial cultures. Based on the specificity and yield, bacterial cultures were selected and successfully generated the glucuronide in sufficient quantity for characterization. Detailed NMR studies were carried out using gradient correlated spectroscopy (COSY), nuclear Overhauser enhancement spectroscopy (NOESY), rotating frame Overhauser enhancement spectroscopy (ROESY), heteronuclear single quantum coherence (HSQC), and heteronuclear multiple bond correlation (HMBC) experiments to assign the ^{1}H and ^{13}C spectra. The nuclear Overhauser effect (NOE) data, combined with the gradient HMBC experiment and molecular modeling, strongly suggest that the point of attachment of the glucuronic acid forms the *N*-glucuronide (2*S*,3*S*,4*S*,5*R*,6*R*)-3,4,5-trihydroxy-6-(5-(4-((1*R*,3*r*,5*S*)-3-hydroxy-8-oxabicyclo[3.2.1]octan-3-yl)-6-((*R*)-3-methylmorpholino)-1*H*-pyrazolo[3,4-*b*]pyridin-1-yl)-1*H*-pyrazol-1-yl)tetrahydro-2*H*-pyran-2-carboxylic acid. This approach represents an efficient tool for glucuronide metabolite synthesis and subsequent characterization.

Materials and Methods

Chemicals. Camonsertib or RP-3500 and camonsertib-d_4 were obtained from Repare Therapeutics (St-Laurent, QC, Canada) with a purity of >99%. A description of the synthetic pathway has been reported by Black et al. (2024). Deuterium oxide, DMSO, formic acid, labetalol hydrochloride and DMSO-d_6 were purchased from Sigma-Aldrich (St. Louis, MO). Hepatocytes thawing media was from BioIVT (Westbury, NY). D-Fructose, HEPES, and Dulbecco's modified Eagle's medium were purchased from Sigma-Aldrich and used to prepare the incubation media. Acetonitrile was purchased from Fisher Scientific (St-Laurent, QC, Canada).

Hepatocyte Incubations. Mixed gender human hepatocytes were purchased from BioIVT (Westbury, NY) and thawed according to the manufacturer's instructions. Camonsertib was incubated at an assay concentration of 10 μM with 1 million cells/ml of human hepatocytes at 37°C. At time points of 0, 120, and 240 minutes, reactions were terminated and extracted by protein precipitation with 5 volumes of acetonitrile. After centrifugation the extracts were diluted 1:1 with water.

Mass Spectrometry. Chromatographic separations and accurate mass measurements were obtained on an UPLC-QTOF MS system that consisted of an Aquity H-class UPLC coupled to a Xevo G2 quadrupole time-of-flight mass spectrometer with electrospray ionization operated in positive mode (Waters Corporation, Milford, MA). High energy acquisition data were also collected using a collision energy ramp of 20–40 eV to generate fragment ions. A lockspray solution of leucine enkephalin was used to ensure mass accuracy. Injections (5 μl) were made onto a BEH C18 column (2 × 50 mm, 1.7 μm; Waters Corporation) eluted at 0.45 ml/min, mobile phase A consisted of water with 0.1% formic acid, and mobile phase B contained acetonitrile with 0.1% formic acid. After a 0.25-minute hold at 5% B, a linear gradient was applied from 5%–70% mobile phase B (0–13 minutes), followed by re-equilibration at 5% B for 2 minutes. For in vitro blood and plasma stability studies, the nominal mass quantitative liquid chromatography tandem mass spectrometry (LC-MS/MS) method used an Ultima system (Waters Corporation) employing positive mode electrospray multiple reaction monitoring transitions of $[M+H]^+$ = 411.1/352.9 (camonsertib), $[M+H]^+$ = 586.6/411.0 (camonsertib glucuronide), and $[M+H]^+$ = 415.1/356.9 (d4-camonsertib internal standard). Reversed-phase high-performance liquid chromatography (HPLC) separations were performed using a Synergi MAX-RP column (2.0 × 150 mm, 4 μm; Phenomenex, Torrance, CA). For recombinant UGT phenotyping studies, positive mode electrospray multiple reaction monitoring transitions of $[M+H]^+$ = 411.3/353.0 (camonsertib) and $[M+H]^+$ = 348.0/205.0 (internal standard 1′ hydroxymidazolam-d4) were obtained using an API4500 system (SCIEX, Framingham, MA). Reversed-phase HPLC separations were

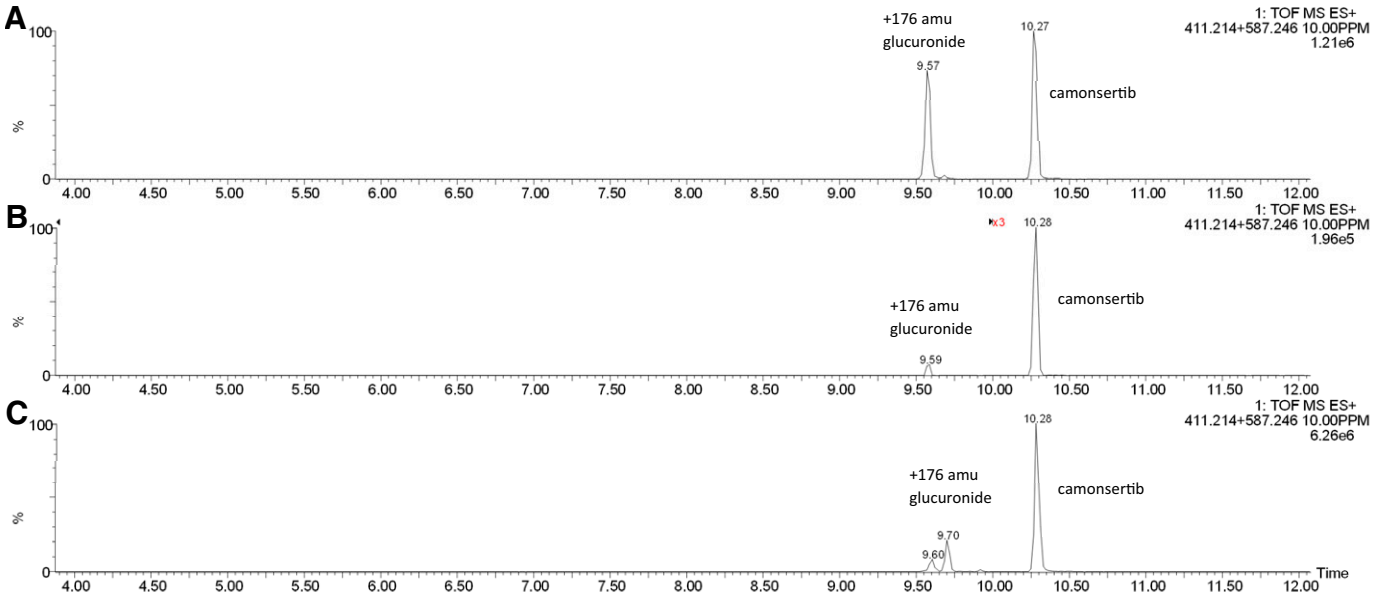

Fig. 2. Extracted-ion chromatogram trace of (A) bacterial Sp288 culture incubations with camonsertib, (B) human hepatocyte incubations with camonsertib (3× magnified in 4- to 10-minute range), and (C) chemical synthesis using a Schmidt glucuronidation procedure.

performed using an Atlantis dC18 column (2.1 × 100 mm, 5 μm; Waters Corporation) on a Shimadazu Nexera X2 liquid chromatograph (Kyoto, Japan).

Preparative Scale Biosynthesis of *N*-Glucuronide–Fermentation. Initial screening studies using 27 microbial strains identified bacterial culture Sp288 as the best producer of camonsertib glucuronide. Uridine diphosphate glucuronic acid cofactor addition was not required for the microbial system. Sp288 is a proprietary bacterial strain of the genera Streptomyces. The confirmation experiment seed flasks (250 ml Erlenmeyer flasks each containing 50 ml of proprietary M3G medium) were each inoculated with 100 μl of Sp288 (from cryo-preserved

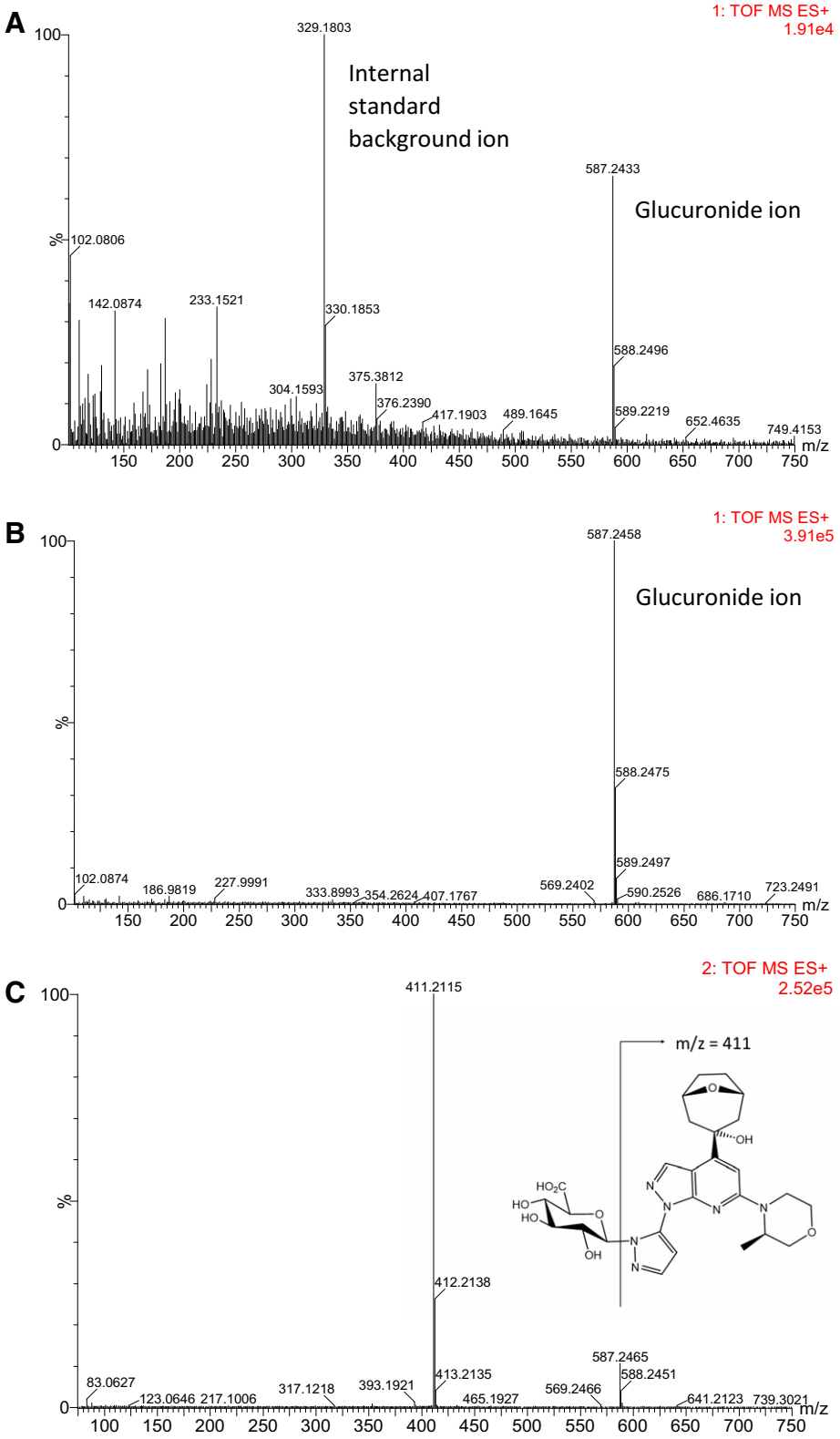

Fig. 3. Accurate mass spectrum of camonsertib glucuronide in (A) human hepatocyte extract, and (B) scale-up from bacterial culture Sp288. (C) High-energy (20–40eV collision energy ramp) accurate mass spectrum of camonsertib glucuronide scale-up from bacterial culture Sp288.

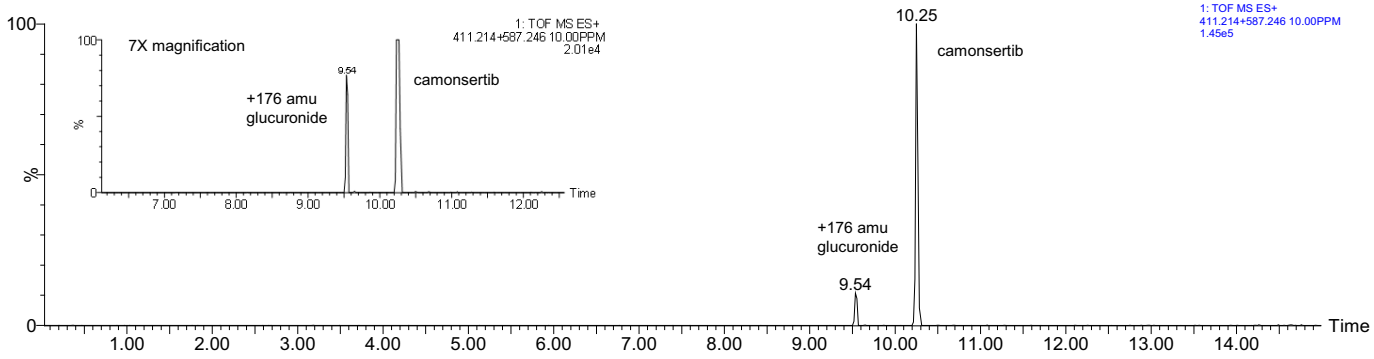

Fig. 4. Extracted-ion chromatogram trace of purified glucuronide spiked into an extract from human hepatocyte incubations with camonsertib. Inset panel scale magnified 7× to demonstrate a single +176 amu chromatographic peak.

glycerol stocks stored over liquid nitrogen) and incubated for 3 days at 27°C, 200 rpm. After the specified growth period, 18 fresh 250 ml Erlenmeyer flasks, each of which contained 50 ml of M3G medium, were each inoculated with 1 ml seed culture and incubated at 27°C and 200 rpm. Flasks were split into three sets of six, with each set further split into three pairs (A and B). After 6 hours growth, the first set of six flasks were dosed with each pair of flasks receiving 100, 250, or 500 mg/l of camonsertib formulated with 20% hydroxypropyl-β-cyclodextrin, respectively. This was repeated for the second set of six flasks after 24 hours and again for the third set of six flasks after 48 hours. A total of 255 mg camonsertib was used in the bacterial incubations. The contents of the A flasks were harvested and frozen, depending on the observed conversion to camonsertib glucuronide. All the remaining flasks were harvested at the end of the experiment and combined with the previous harvests for subsequent extraction and purification.

Semipreparative HPLC Purification. The combined harvested material was thawed at 40°C, centrifuged, and the supernatant decanted. The supernatant was adsorbed onto a column of Diaion HP20 resin (2 cm diam. × 42 cm, 135 ml, Mitsubishi Chemical Corporation), previously washed with MeOH and re-equilibrated in H_2O. The column was then washed with H_2O until the effluent became pale yellow. Thereafter, the column was eluted with MeCN/H_2O mixtures (150 ml, v/v) 20/80, 40/60, 60/40, 80/20 and finally with MeCN (200 ml). The bulk of the glucuronide eluted in the 20/80 and 40/60 fractions. However, approximately 30% of the glucuronide was not retained on the column and was present in the unbound fraction and H_2O wash. The glucuronide-containing aqueous wash and unbound fractions were recycled back through the same HP20 capture/elution steps; all materials containing the target glucuronide were combined and lyophilized.

The lyophilizate was chromatographed over an Atlantis T3 Prep OBD column (5 μm, 19 × 100 mm; Waters Corporation) with a MeCN/H_2O gradient (both solvents containing 0.1% formic acid) starting at 10/90, holding for 1 minute, increasing to 20/80 over 1 minute, then increasing further to 24/76 over another 8 minutes (t = 10 minutes), followed by wash and re-equilibration steps, all at a flow rate of 17 ml/min. The glucuronide eluted at 8.0 minutes, and the fractions containing the target were lyophilized. The lyophilizate was dissolved in MeOH and subjected to size exclusion chromatography over Sephadex LH20, eluting with MeOH as follows: Sephadex LH20 was pre-swollen in 100% MeOH and transferred to a glass column to give a total bed dimension of 150 × 22 mm. The sample was loaded onto the LH20 column in a minimal volume of MeOH and eluted under gravity with MeOH. The target-containing fractions were evaporated under reduced pressure and lyophilized to give a light-yellow oil. This oil was redissolved in MeOH (1.5 ml) and fractionated over a Xbridge BEH C18 column (30 × 100 mm + 30 × 10 mm guard column; Waters Corporation) eluting with a flow rate of 40 ml/min as follows; the gradient started at 90%/5%/5% (H_2O/MeCN/200 mM ammonium bicarbonate) and increased to 70%/25%/5% over 11 minutes, followed by wash and re-equilibration steps with the target glucuronide eluting between 8.8 and 10.2 minutes. Target-containing fractions were pooled, evaporated under reduced pressure to remove MeCN and lyophilized to give 25.1 mg of the glucuronide as a white powder. Overall yield was estimated to be 9.8% when the resulting glucuronide product was pooled from all the dose escalations and incubation time conditions.

NMR Spectroscopy. Proton and carbon NMR assignments for camonsertib were obtained on a Varian Inova spectrometer (Palo Alto, CA) operating at 400 MHz equipped with a 5 mm AutoSwitchable probe. Data were acquired with OpenVnmrJ 3.1. A total of 18 mg of camonsertib was dissolved in 0.7 ml of DMSO-d_6 and placed in a 5-mm tube. Proton and carbon NMR assignments for camonsertib glucuronide were obtained on a Bruker Avance II spectrometer (Billerica, MA) operating at 500 MHz equipped with a 5-mm BBI probe. Data were acquired with TopSpin 2.1. A total of 10 mg of camonsertib glucuronide was dissolved in 0.7 ml of DMSO-d_6 and placed in a 5-mm tube. In all cases, chemical shifts were referenced to the DMSO solvent signal at δ = 2.50 ppm for ^{1}H and δ = 39.51 ppm for ^{13}C. NOESY and ROESY experiments were acquired with a 1.0 second and 0.3 second mixing time, respectively. HSQC spectra were multiplicity edited.

Molecular Modeling. Conformational sampling was performed using the Molecular Operating Environment (MOE), version 2020.09 (Chemical Computing Group ULC, Montreal, QC, Canada). In silico predictions of the site of glucuroni-

TABLE 1

Proton and carbon NMR assignments for camonsertib (Fig. 1) in DMSO-d_6 solution (~20 mg/0.7 ml)

Proton reference: DMSO-d_5 at δ = 2.50 ppm; carbon reference: DMSO-d_6 at δ = 39.51 ppm. Spectra were obtained on a Varian Inova spectrometer operating at 400 MHz. Multiplicities are s (singlet), d (doublet), and t (triplet). Note that the protons labeled "syn" are on the same side of the bicyclic ring as the bridging oxygen, whereas the protons labeled "anti" are on the side of the bicyclic ring opposite to the bridging oxygen.

Position	δH (ppm)	Multiplicity J_H (Hz)	Proton Count	δC (ppm)
11-NH	12.80	s	1H	—
3	8.05	s	1H	133.61
4	—	—	—	155.97
5	6.80	s	1H	99.27
6	—	—	—	157.95
8	—	—	—	150.49
9	—	—	—	105.70
12	7.83	t, J = 1.7, 1.7	1H	129.48
13	6.79	t, J = 1.8, 1.8	1H	97.12
14	—	—	—	147.12
1′, 5′	4.45	m	2H	73.18
2′,4′ syn	2.37	m	2H	43.05
2′,4′ anti	1.77	d, J = 14.0	2H	—
3′	—	—	—	71.48
3′-OH	5.34	s	1H	—
6′,7′ syn	2.36	m	2H	28.33
6′,7′ anti	1.84	m	2H	—
2″eq	3.77	d, J = 11.3	1H	70.48
2″ax	3.64	dd, J = 11.3, 2.6	1H	—
3″	4.43	m	1H	47.31
3a″	1.20	d, J = 6.7	3H	12.89
5″eq	4.03	dd, J = 13.8, 3.1	1H	39.60
5″ax	3.18	ddd J = 12.9, 12.9, 3.6	1H	—
6″eq	3.97	dd, J = 11.5, 2.8	1H	66.24
6″ax	3.49	ddd, J= 11.9, 11.9, 2.6	1H	—

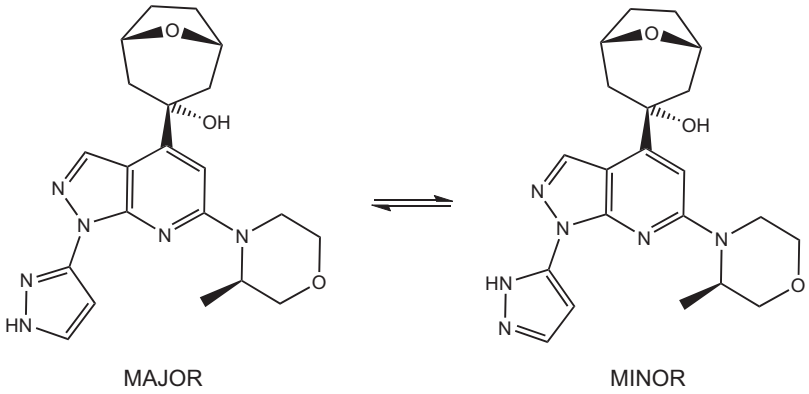

Fig. 5. Proposed tautomeric forms of ATR inhibitor camonsertib observed in DMSO-d_6.

dation were evaluated using both Meteor Nexus v.3.1.0 (Lhasa Limited, Leeds, UK) and MedChem Designer v6.3.0.4 (Simulations Plus, Lancaster CA).

Recombinant UGT Enzymes. Recombinant human UGT enzymes were supplied by Corning (Corning, NY). Camonsertib was incubated at either 0.1 or 1 μM with recombinant human UGT enzymes (rUGT1A1, rUGT1A3, rUGT1A4, rUGT1A6, rUGT1A7, rUGT1A8, rUGT1A9, rUGT1A10, rUGT2B4, rUGT2B7, rUGT2B10, rUGT2B15, and rUGT2B17) at a concentration of 1 mg microsomal protein/ml. Incubations were conducted at 37°C for 120 minutes and terminated with the addition of acetonitrile. Samples were analyzed by LC-MS/MS to quantify the camonsertib concentration remaining.

Results

Human hepatocyte incubations with camonsertib showed low rates of metabolic turnover, revealing the presence of phase I oxidative metabolites but also a single direct glucuronide metabolite. The site of glucuronidation can be challenging to pinpoint by LC-MS/MS alone when several plausible functional sites are present in the molecule, because MS/MS fragmentation typically cleaves the glucuronide back to the parent molecule, providing very little structural information (Guo et al., 2022). Interestingly, using Meteor Nexus, the proposed metabolic sites for the glucuronide included the tertiary alcohol and both nitrogen atoms of the pyrazole, whereas MedChem Designer predicted only conjugation on the tertiary alcohol. Therefore, to more accurately reveal the location of the glucuronide, NMR elucidation of a purified isolate was deemed necessary. Additionally, purified material was further used to characterize stability and serve as a reference standard for quantitation purposes.

Initial screening studies were performed to evaluate the most efficient option to generate sufficient quantities of the glucuronide. Approaches using a number of chemical synthesis conditions, incubations with S9 liver fractions derived from a panel of mammalian species and multiple bacterial cultures were evaluated. The bacterial culture Sp288 was identified as the optimal producer of a single camonsertib glucuronide peak with the same retention time as the human hepatocyte incubations (Fig. 2, A and B). Application of chemical synthesis using a Schmidt trichloroacetimidate glycosylation procedure (Schmidt and Michel, 1980; Schmidt and Kinzy, 1994) produced two

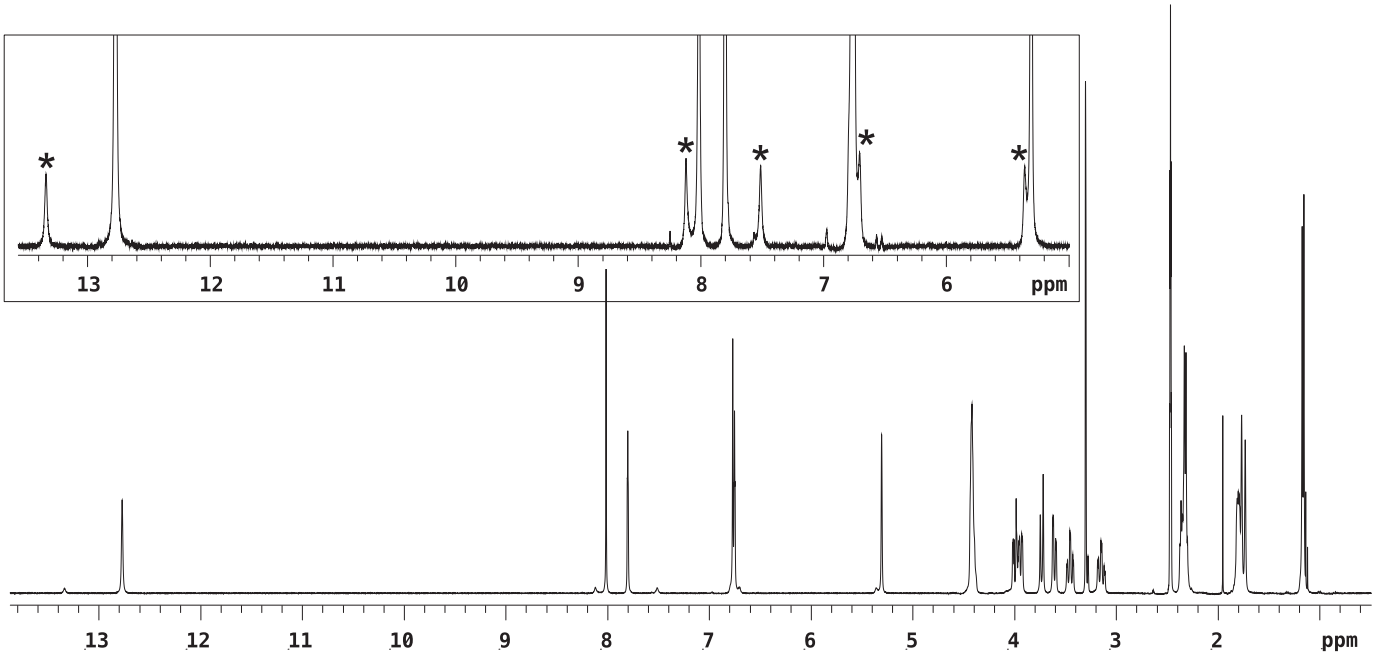

Fig. 6. ^{1}H NMR spectrum of camonsertib in DMSO-d6. The minor isomer peaks are identified with an asterisk (*) in the inset.

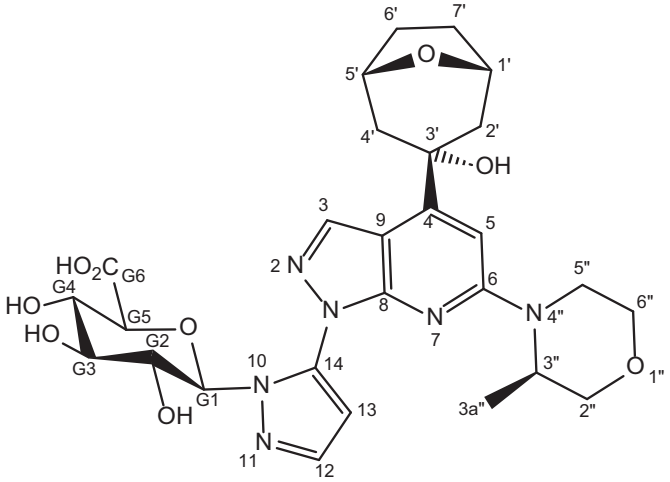

Fig. 7. Glucuronide metabolite of camonsertib.

glucuronide peaks (+176 amu) in low abundance. Although not specific to the single glucuronide in human hepatocyte incubations, these chemical synthesis products helped demonstrate the ability of the chromatography conditions to resolve potential glucuronide isomers (Fig. 2C). We hypothesized these two peaks to be the glucuronide regioisomers resulting from attachment to either of the two nitrogen atoms of the pyrazole based on the chemical synthesis approach employed.

Bacterial culture Sp288 was selected for larger scale glucuronide biosynthesis by incubating with camonsertib. Using solid phase extraction and preparative chromatography, glucuronide-containing fractions were lyophilized, and the resulting material from this step provided 25.1 mg glucuronide at >95% purity by LC-UV-evaporative light scattering detection. The accurate mass of the biosynthetic glucuronide matched that of the human hepatocyte incubation sample injection (Fig. 3, A and B), both at <5 ppm of the expected accurate mass. Fragmentation of the isolated camonsertib glucuronide did not provide any additional structural information since it fragmented to a single mass-to-charge ratio = 411.2115 using a high-energy ramped MS acquisition (Fig. 3C). Figure 4 shows the extracted ion-chromatogram of the purified glucuronide material spiked into an extract of the human hepatocyte incubations of camonsertib. A single, sharp glucuronide peak at 9.54 minutes was observed, confirming the correct human hepatocyte-generated metabolite was isolated from bacterial culture Sp288.

Using a reference standard of camonsertib and the purified glucuronide material, detailed NMR studies were carried out to resolve the chemical structure. First, gradient COSY, NOESY, HSQC, and HMBC experiments (Supplemental Figs. 3–6), were used to assign the ^{1}H (Supplemental Fig. 1), and ^{13}C spectra (Supplemental Fig. 2), for camonsertib, and the assignments are shown in Table 1. For camonsertib in DMSO-d_6, the NMR data suggests the presence of pyrazole tautomers in an 8:1 ratio as depicted in Figs. 5 and 6 where ^{1}H NMR signals of the minor isomer are highlighted in the spectrum inset.

NMR studies were carried out on the glucuronide metabolite of camonsertib, the structure was assigned as depicted in Fig. 7. Gradient COSY, NOESY, ROESY, HSQC, and HMBC experiments (Supplemental Figs. 9–13) were used to assign the ^{1}H (Supplemental Fig. 7) and ^{13}C spectra (Supplemental Fig. 8), and the assignments are shown in Table 2. Note that the protons labeled "syn" are on the same side of the bicyclic ring as the bridging oxygen, whereas the protons labeled "anti" are on the side of the bicyclic ring opposite to the bridging oxygen.

Discussion

Analysis of the gradient HMBC spectrum (Supplemental Fig. 11) of the glucuronide adduct showed a cross peak between the anomeric proton of the glucuronic acid (position G1) and carbon 14 in Fig. 7. An expansion of the appropriate region of the HMBC experiment is shown in Fig. 8. With three-bond HMBC correlations being the most likely to be observed, this would suggest that the point of attachment of the glucuronide is at the pyrazole nitrogen of camonsertib labeled 10 (Fig. 7). However, in the unlikely case that the cross peak arises from a four-bond correlation, it is possible that the point of attachment is at nitrogen 11. It is not possible to conclusively distinguish between these two options from the gradient HMBC experiment alone. Furthermore, the HMBC cross peak between the anomeric hydrogen G1 and carbon 14 eliminates the possibility of glucuronidation at 3′-OH position. No other cross peaks between the parent molecule and the glucuronic acid were observed. Based on the coupling constant 9.0 Hz observed for the anomeric proton labeled G1, this proton is in the axial orientation, indicating the glucuronide attachment in a β configuration which is consistent with its formation from a biologic system. Analysis of the NOESY (Supplemental Fig. 10) and ROESY (Supplemental Fig. 9) spectra of the glucuronide adduct showed a cross peak between the protons at positions labeled G1 and G3 in Fig. 7. An expansion of the appropriate region of the NOESY experiment is shown in Fig. 9. To address the potential for glucuronide attachment at either of the pyrazole nitrogen atoms (labeled 10

TABLE 2

Proton and carbon NMR assignments for camonsertib glucuronide (Fig. 7) in DMSO-d6 solution (~10 mg/0.7 ml)

Proton reference: DMSO-d_5 at δ = 2.50 ppm; carbon reference: DMSO-d_6 at δ = 39.51 ppm. Spectra were obtained on a Bruker Avance II spectrometer operating at 500 MHz. Multiplicities are s (singlet), d (doublet), and t (triplet).

Position	δH (ppm)	Multiplicity J_H (Hz)	Proton Count	δC (ppm)
3	8.21	s	1H	135.68
4	—	—	—	156.29
5	6.82	s	1H	99.88
6	—	—	—	158.26
8	—	—	—	151.72
9	—	—	—	105.36
12	7.70	d, J = 1.7	1H	138.97
13	6.60	d, J = 1.8	1H	100.57
14	—	—	—	137.43
1′, 5′	4.46	m	2H	73.16
2′,4’ syn	2.38	m	2H	43.10
2′,4′ anti	1.81	d, J = 14.5	2H	—
3′	—	—	—	71.52
6′,7′ syn	2.36	m	2H	28.29
6′,7′ anti	1.84	m	2H	—
2″eq	3.74	d, J = 11.3	1H	70.39
2″ax	3.62	dd, J = 11.4, 2.9	1H	—
3″	4.41	m	1H	47.30
3a″	1.19	d, J = 6.7	3H	13.05
5″eq	4.07	d, J = 13.4	1H	39.57
5″ax	3.12	ddd J = 13.3, 13.3, 4.0	1H	—
6″eq	3.93	dd, J = 11.4, 3.4	1H	66.26
6″ax	3.46	ddd, J = 11.9, 11.9, 3.0	1H	—
G1	5.50	d, J = 9.0	1H	85.32
G2	3.96	t, J = 8.9	1H	71.11
G3	3.20	d, J = 8.8	1H	77.53
G4	3.26	d, J = 9.0	1H	71.87
G5	3.37	d, J = 9.7	1H	76.79
G6	—		—	171.42

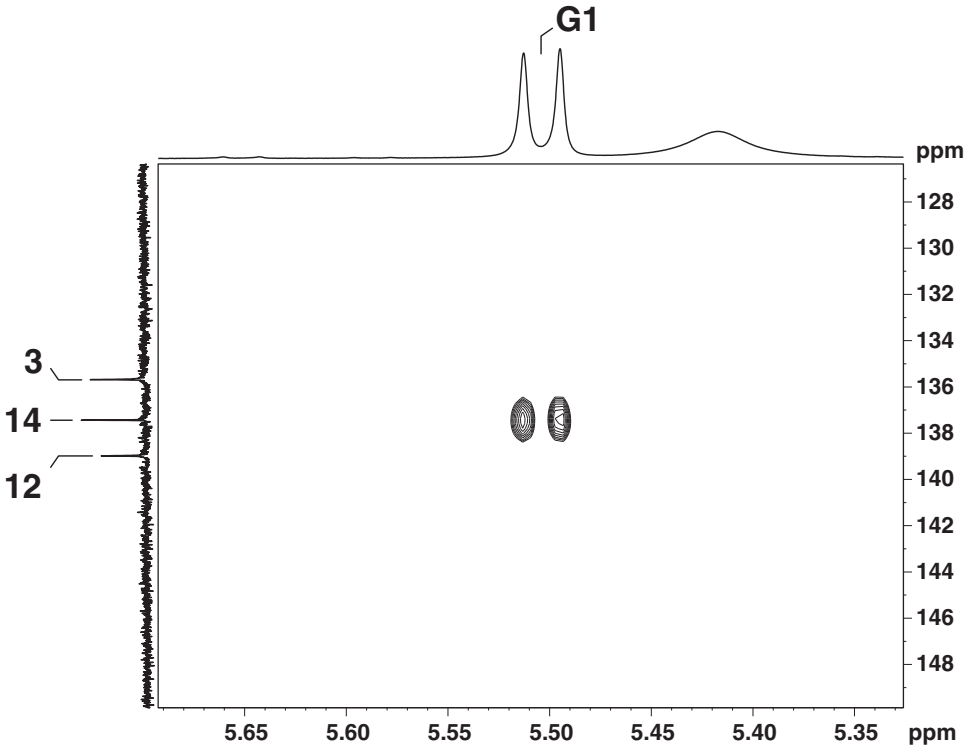

Fig. 8. Expansion of the gradient HMBC spectrum highlighting the correlation between the anomeric glucuronide proton and C14.

and 11), molecular modeling studies were performed with the glucuronide adduct at either position to estimate proton stances and assist with interpretation of NOE cross peaks in NMR data. "LowModeMD" molecular dynamics simulations with enhanced sampling were performed within the molecular operating environment (Molecular Operating Environment, 2020), using the default run parameters. The glucuronide anomeric proton would need to be in close proximity (4.1 Å [3.9–4.2]) to the proton at position labeled 3 to show an NOE cross peak, which is consistent with

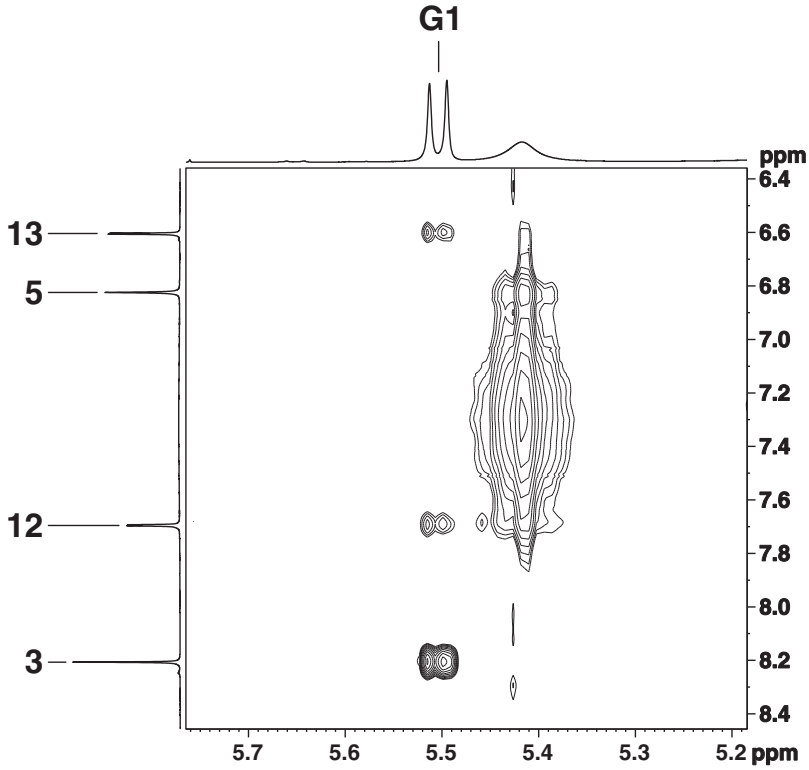

Fig. 9. Expansion of the NOESY spectrum highlighting the correlations between the anomeric glucuronide proton and H13, H12, and H3.

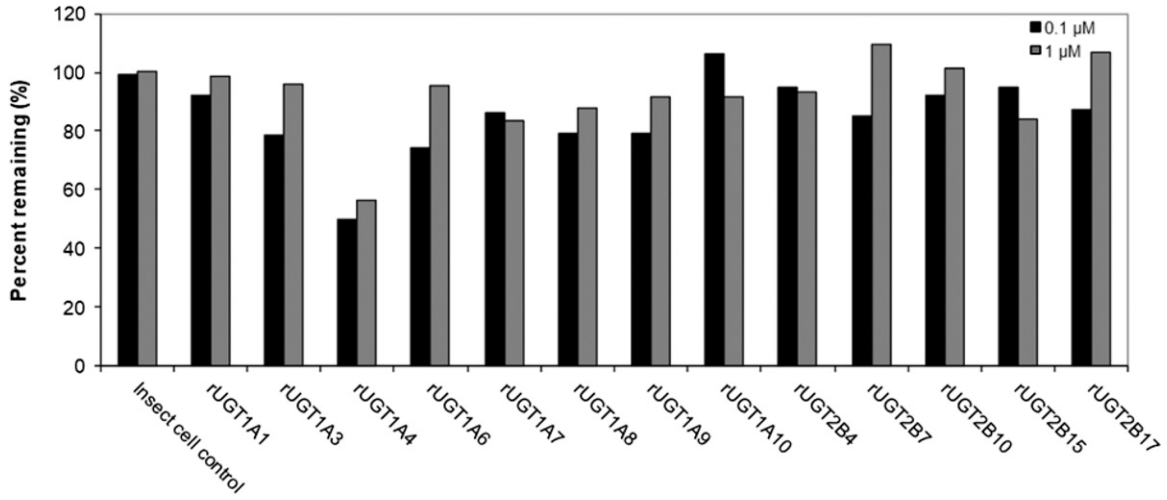

Fig. 10. Percent of camonsertib remaining after incubations with a panel of recombinant human UGTs (1 mg microsomal protein/ml).

the distances observed in the LowModeMD simulation with the adduct at position labeled N10 in Fig. 7. However, if the glucuronidation occurred at position N11, the distance between the anomeric proton and proton at position 3 would be too great (approximately 7.3–8.7 Å) to expect to observe an NOE (Rahman et al., 2016). The combination of the NOE data and the gradient HMBC experiment (Supplemental Fig. 11) strongly suggests that the point of attachment of the glucuronic acid forms the *N*-glucuronide depicted in Fig. 7.

Direct *N*-glucuronides are observed with drugs containing amino groups or aromatic nitrogen heterocycles, and examples include lamotrigine (Milosheska et al., 2016), diphenhydramine (Fischer and Breyer-Pfaff 1997), carbamazepine (Staines et al., 2004), amitriptyline, and cyclobenzaprine (Mastrianni et al., 2016). Importantly, no reported safety issues specifically ascribed to *N*-glucuronides have been cited (Kerns and Di, 2008; Kaivosaari 2011). It has been generally accepted that *N*-glucuronides are more readily produced in guinea pigs, rabbits, humans, and non-human primates compared with either rats or dogs, although exceptions should be noted (Chiu and Huskey 1998; Uldam et al., 2011). The UGT isoforms that have been implicated in the formation of *N*-glucuronides in humans include UGT1A4, UGT2B10, UGT2B7, UGT1A1, and UGT1A3, as well as UGT1A6 and UGT1A9 (Kaivosaari 2011; Uldam et al., 2011). Studies using recombinant UGT enzymes showed low turnover but suggested camonsertib is a substrate of UGT1A4. However, contributions from UGT1A3, UGT1A6, UGT1A8, and UGT1A9 were also detected (Fig. 10), where at least 20% loss of camonsertib was observed after a 120-minute incubation at either 0.1 or 1μM.

Despite reports that *N*-glucuronides are more stable than acyl glucuronides at physiologic conditions (Guo et al., 2022), stability studies were undertaken with the glucuronide of camonsertib. The *N*-glucuronide was evaluated for short-term stability in human whole blood (Table 3) and human plasma (Table 4), with the goal of identifying potential bioanalytical/pharmacokinetic measurement issues specifically related to cleavage back to camonsertib during sample processing. Such early knowledge is critical prior to first-in-human studies and formal method validation, where stabilizers and optimized storage conditions can be implemented prior to generating first-in-human pharmacokinetic data. Under both experimental conditions, the level of detectable camonsertib was unchanged from the T_0 sample regardless of the processing temperature and represented at most ~0.02% of camonsertib likely present as a trace impurity in the originally isolated glucuronide reference material.

TABLE 3

Percentage of camonsertib detected from human whole blood spiked with 2000 ng/ml camonsertib *N*-glucuronide

Replicate	T_0	Room Temperature (1 h)	37°C (1 h)
1	0.022%	0.022%	0.022%
2	0.020%	0.020%	0.021%
3	0.020%	0.021%	0.023%
Mean	0.021%	0.021%	0.022%

The *N*-glucuronide was deemed stable under typical bioanalytical sample processing conditions for formal method validation and eventual clinical sample analysis of camonsertib. Long-term plasma storage stability will be studied separately if substantial quantities are detected in human plasma or alternatively evaluated as part of incurred sample reanalysis sampling protocols by measurement of camonsertib. The chromatography indicates the metabolite is well-separated from camonsertib and therefore does not pose any concerns from in-source fragmentation interference during LC-MS/MS analysis.

An efficient, cost-effective approach was employed to successfully produce, identify, and characterize an *N*-glucuronide metabolite of camonsertib that was observed in human hepatocyte incubations. This approach represents a cost-effective tool for metabolite synthesis, since advanced compounds are usually optimized for low clearance, and typical in vitro systems are often not efficient metabolite producers for scale-up activities. The effort enabled bioanalytical characterization to ensure accurate quantitation of camonsertib prior to first-in-human studies. Furthermore, generating 25 mg reference standard material of a metabolite can be useful for further bioanalytical assay development, stability studies, or metabolism experiments where quantitative measurements are needed, especially MS-based methods where differences in ionization efficiency preclude estimates based on parent compound response (Hatsis et al., 2017). Generation of a sufficiently pure material was paramount for detailed NMR structural elucidation studies, which indicated the most likely point of attachment of the glucuronic acid results in the formation of the *N*-glucuronide described in Fig. 7.

TABLE 4

Percentage of camonsertib detected from K_2EDTA human plasma spiked with 1000 ng/mL camonsertib *N*-glucuronide

		Ice Bath		Room Temperature		37°C	
Replicate	T_0	3 h	6 h	3 h	6 h	3 h	6 h
1	0.011%	0.015%	0.011%	0.012%	0.014%	0.014%	0.015%
2	0.012%	0.009%	0.015%	0.011%	0.012%	0.012%	0.013%
3	0.011%	0.011%	0.009%	0.012%	0.014%	0.014%	0.013%
Mean	0.011%	0.012%	0.012%	0.012%	0.013%	0.013%	0.014%

Acknowledgments

The authors thank M. Diallo for assistance with hepatocyte incubations and Xenotech Inc. for performing UGT phenotyping studies.

Data Availability

The authors declare that all the data supporting the findings of this study are available within the paper and its Supplemental Material. Additional data requests may be directed to the corresponding author.

Authorship Contributions

Participated in research design: Papp, Trimble, Fretland, Kvaerno, Perryman, Black.

Conducted experiments: Papp, Trimble, Manohar, Phipps, Kvaerno, Reynolds.

Performed data analysis: Papp, Trimble, Manohar, Phipps, Perryman, Reynolds.

Wrote or contributed to the writing of the manuscript: Papp, Trimble, Fretland, Kvaerno, Perryman, Black.

References

Bailey MJ and Dickinson RG (2003) Acyl glucuronide reactivity in perspective: biological consequences. *Chem Biol Interact* **145**:117–137.

Black WC, Abdoli A, An X, Auger A, Beaulieu P, Bernatchez M, Caron C, Chefson A, Crane S, Diallo M, et al. (2024) Discovery of the Potent and Selective ATR Inhibitor Camonsertib (RP-3500). *Journal of medicinal chemistry* **67**:2349–2368.

Bradshaw PR, Athersuch TJ, Stachulski AV, and Wilson ID (2020) Acyl glucuronide reactivity in perspective. *Drug Discov Today* **25**:1639–1650.

Chiu SHL and Huskey SW (1998) Species differences in N-glucuronidation. *Drug Metab Dispos* **26**:838–847.

Fischer D and Breyer-Pfaff U (1997) Variability of diphenhydramine N-glucuronidation in healthy subjects. *Eur J Drug Metab Pharmacokinet* **22**:151–154.

Guo Y, Shah A, Oh E, Chowdhury SK, and Zhu X (2022) Determination of acyl-, *O*-, and *N*-glucuronide using chemical derivatization coupled with liquid chromatography-high-resolution mass spectrometry. *Drug Metab Dispos* **50**:716–724.

Hatsis P, Waters NJ, and Argikar UA (2017) Implications for metabolite quantification by mass spectrometry in the absence of authentic standards. *Drug Metab Dispos* **45**:492–496.

Kaivosaari S (2011) *N-Glucuronidation of Drugs and Other Xenobiotics*. Doctoral dissertation, University of Helsinki, Helsinki, Finland.

Kaivosaari S, Finel M, and Koskinen M (2011) N-glucuronidation of drugs and other xenobiotics by human and animal UDP-glucuronosyltransferases. *Xenobiotica* **41**:652–669.

Keating KA, McConnell O, Zhang Y, Shen L, Demaio W, Mallis L, Elmarakby S, and Chandrasekaran A (2006) NMR characterization of an S-linked glucuronide metabolite of the potent, novel, nonsteroidal progesterone agonist tanaproget. *Drug Metab Dispos* **34**:1283–1287.

Kerdpin O, Elliot DJ, Mackenzie PI, and Miners JO (2006) Sulfinpyrazone C-glucuronidation is catalyzed selectively by human UDP-glucuronosyltransferase 1A9. *Drug Metab Dispos* **34**:1950–1953.

Kerns EH and Di L (2008) *Drug-Like Properties: Concepts, Structure Design and Methods: from ADME to Toxicity Optimization*, Academic Press, Amsterdam.

Mastrianni KR, Lee LA, Brewer WE, Dongari N, Barna M, and Morgan SL (2016) Variations in enzymatic hydrolysis efficiencies for amitriptyline and cyclobenzaprine in urine. *J Anal Toxicol* **40**:732–737.

Milosheska D, Lorber B, Vovk T, Kastelic M, Dolžan V, and Grabnar I (2016) Pharmacokinetics of lamotrigine and its metabolite N-2-glucuronide: Influence of polymorphism of UDP-glucuronosyltransferases and drug transporters. *Br J Clin Pharmacol* **82**:399–411.

Molecular Operating Environment (2023) Molecular Operating Environment (MOE), 2022.02. Chemical Computing Group ULC, Montreal, QC, Canada.

Rahman AU, Choudhary MI, and Wahab A (2016) *Nuclear Overhauser Effect. Solving Problems with NMR Spectroscopy*, 2nd ed, pp 227–264, Academic Press, Oxford.

Roulston A, Zimmermann M, Papp R, Skeldon A, Pellerin C, Dumas-Bérube É, Dumais V, Dorich S, Fader LD, Fournier S et al. (2022) RP-3500: a novel, potent, and selective ATR inhibitor that is effective in preclinical models as a monotherapy and in combination with PARP inhibitors. *Mol Cancer Ther* **21**:245–256.

Sadeque AJM, Usmani KA, Palamar S, Cerny MA, and Chen WG (2012) Identification of human UDP-glucuronosyltransferases involved in N-carbamoyl glucuronidation of lorcaserin. *Drug Metab Dispos* **40**:772–778.

Schmidt RR and Kinzy W (1994) Anomeric-oxygen activation for glycoside synthesis: the trichloroacetimidate method. *Adv Carbohydr Chem Biochem* **50**:21–123.

Schmidt RR and Michel J (1980) Facile Synthesis of α- and β- O -Glycosyl Imidates; Preparation of Glycosides and Disaccharides. *Angewandte Chemie International Edition in English* **19**: 731–732.

Staines AG, Coughtrie MWH, and Burchell B (2004) N-glucuronidation of carbamazepine in human tissues is mediated by UGT2B7. *J Pharmacol Exp Ther* **311**:1131–1137.

Uldam HK, Juhl M, Pedersen H, and Dalgaard L (2011) Biosynthesis and identification of an N-oxide/N-glucuronide metabolite and first synthesis of an N-O-glucuronide metabolite of Lu AA21004. *Drug Metab Dispos* **39**:2264–2274.

Wang L, Zhang D, Swaminathan A, Xue Y, Cheng PT, Wu S, Mosqueda-Garcia R, Aurang C, Everett DW, and Humphreys WG (2006) Glucuronidation as a major metabolic clearance pathway of 14c-labeled muraglitazar in humans: metabolic profiles in subjects with or without bile collection. *Drug Metab Dispos* **34**:427–439.

Yang G, Ge S, Singh R, Basu S, Shatzer K, Zen M, Liu J, Tu Y, Zhang C, Wei J et al. (2017) Glucuronidation: driving factors and their impact on glucuronide disposition. *Drug Metab Rev* **49**:105–138.

Yap TA, Fontana E, Lee EK, Spigel DR, Højgaard M, Lheureux S, Mettu NB, Carneiro BA, Carter L, Plummer R et al. (2023) Camonsertib in DNA damage response-deficient advanced solid tumors: phase 1 trial results. *Nat Med* **29**:1400–1411.

Yuan L, Sophia Xu X, and Ji QC (2020) Challenges and recommendations in developing LC-MS/MS bioanalytical assays of labile glucuronides and parent compounds in the presence of glucuronide metabolites. *Bioanalysis* **12**:615–624.

Address correspondence to: Robert Papp, Drug Metabolism and Pharmacokinetics, Repare Therapeutics, 7171 Frederick Banting, St-Laurent, Quebec, Canada. E-mail: rpapp@reparerx.com